Technical Sciences, 2025, 28, 265–279

UNIWERSYTET WARMIŃSKO-MAZURSKI W OLSZTYNIE

Yearbook peer-reviewed scientific journal
ISSN 1505-4675
e-ISSN 2083-4527
TECHNICAL SCIENCES
Homepage: https://czasopisma.uwm.edu.pl/index.php/ts/

DOI: https://doi.org/10.31648/ts.11953

THE EFFECT OF SAMPLE DISPLACEMENT ON X-RAY DIFFRACTION RESULTS IN BRAGG-BRENTANO GEOMETRY

Karol Tyc

ORCID: 0009-0002-0086-0708
Department of Materials and Machines Technology
University of Warmia and Mazury in Olsztyn

Received 29 October 2025, accepted 24 November 2025, 18 December 2025

K e y w o r d s: X-ray diffraction (XRD); Bragg-Brentano geometry; sample displacement; XRD geometric errors.

A b s t r a c t

The aim of the study was to investigate the effect of vertical displacement of the sample on the results of X-ray diffraction (XRD) in Bragg-Brentano geometry. Measurements were performed on an S275JR steel sample using a Phaser D2 diffractometer (Cu Kα, λ = 1.541874 [Å]) with a step size of 2θ = 0.01°. The shifts in the positions of the 2θ peaks and half-widths (FWHM) were analyzed. A comparison between the theoretical model and experimental peak shifts has been calculated. The lattice constant was determined using the Nelson-Riley method, the crystallite size using the Scherrer method, and the parameters using the Williamson-Hall method. A vertical displacement of 1 mm produced an approximately 0.8° shift of the (110) peak. Based on the diffraction data, the lattice parameter was determined using the Nelson-Riley extrapolation method (2.8643-2.8678 [Å]), the crystallite size was evaluated using the Scherrer method (110-260 [Å], with the largest value for the (110) peak), and lattice distortions were assessed using the Williamson–Hall approach (approx. 0.26-0.30[%]). The results highlight the significance of precise sample positioning, as even a small displacement can lead to noticeable errors in peak locations and consequently in the derived structural parameters.

Correspondence: Karol Tyc, Katedra Technologii Materiałów i Maszyn, Wydział Nauk Technicznych, Uniwersytet Warmińsko-Mazurski, ul. Oczapowskiego 11, 10-719 Olsztyn; e-mail: karol.tyc@uwm.edu.pl

Introduction

X-ray diffraction (XRD) is a fundamental technique for determining crystal structure parameters, identifying phases, and evaluating microstructural features of materials, such as crystallite size and internal stresses. XRD applications include both basic research and quality control in industry (e.g., metallurgy, coatings, electrochemical materials, pharmaceuticals), where diffractometric results enable the evaluation of composition, type-III stresses, or the presence of undesirable crystal forms (HARRINGTON, SANTISO 2021). The precision and accuracy of XRD results depend significantly on the measurement geometry and the correct positioning of the sample relative to the goniometer axis, known as the Bragg-Brentano geometry (Fig. 1). This is the classical symmetrical reflection arrangement. The X-ray beam strikes the flat surface of the sample at an angle θ to the sample plane and is scattered at the same angle, while the detector records scattered radiation at an angle 2θ relative to the incident beam. During the measurement, the angle of incidence and the angle of the detector change in a coupled manner so that Bragg's condition is satisfied for successive lattice planes. This allows the detector to record intensity as a function of the diffraction angle (CLINE 2014).

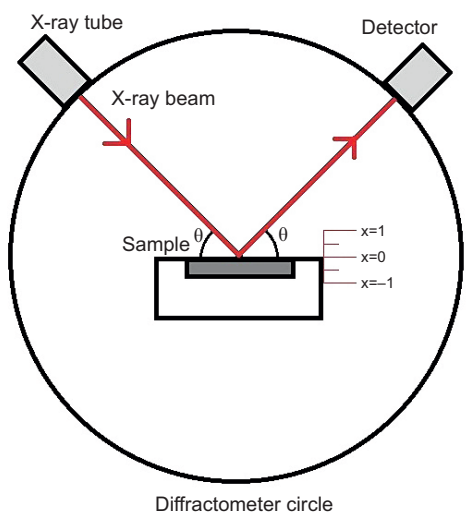

Fig. 1. Bragg-Brentano geometry
Source: Self-made – own source.

In Bragg-Brentano geometry the X-ray source, the sample surface and the detector must lie on the same focusing circle; a vertical displacement of the sample therefore changes the effective point of incidence of the beam relative to the diffractometer radius. A simple geometric derivation shows that, to first order for small displacements, the resulting shift of the recorded diffraction angle [rad.] can be written as (1).

$$\Delta(2\theta) = -2s\frac{\cos\theta}{R} \tag{1}$$

where:

θ – reflection angle [rad.].

s – displacement of the sample [mm]

R – radius of the goniometer circle [mm]

The formula implies two important, experimentally observed facts: the angular shift scales approximately linearly with the displacement s, and the shift is largest at low Bragg angles because of the $\cos\theta$ dependence. If the sample is shifted vertically, the geometric condition is violated and a shift in the angles of maximum reflections (change in the position of 2θ peaks) and possible distortion of the line shape are observed (CULLITY 2014, WEIDENTHALER 2011, KRIEGNER 2015).

In addition to sample displacement, other geometric sources of error may occur, including axial divergence, imperfect flatness of the sample surface, sample transparency (beam penetration through a thin sample), and the use of a simple (linear) detector that does not geometrically fit the focal circle. The aim of this work is to investigate the effect of sample displacement on the recorded XRD spectra, which will allow us to assess the significance of this error and its consequences for the interpretation of crystallographic data.

Materials and methods

Materials

The material investigated in this study was low-carbon structural steel S275JR. The sample surface was prepared for X-ray diffraction measurements in accordance with ASTM E975-13. The chemical composition of the steel (maximum permitted values according to EN 10025-2) is shown in Table 1.

Table 1

Chemical composition of S275JR steel

Element	Carbon	Manganese	Silicon	Phosphorus	Sulfur	Nitrogen	Copper
Content [%]	0.210	1.500	–	0.035	0.035	0.012	0.550

Source: ASTM E975-13.

Experimental setup

XRD measurements were carried out using a Bruker Phaser D2 diffractometer equipped with Cu Kα radiation (mean wavelength $\lambda = 1.541874$ [Å]) and goniometer radius equal 140 mm. Scans were recorded with a step size of 0.01° in 2θ and a counting time of 1 s per step. To introduce controlled vertical displacements, spacers (washers) made of the same steel grade were used. For correct Bragg-Brentano focusing, the sample surface must be positioned at a height of 6 mm, which corresponds to the goniometer rotation axis; this reference (proper) position is denoted as x = 0 and all intentional height shifts are reported relative to this datum. The sample surfaces were set at heights of 5, 5.5, 6, 6.5, and 7 mm.

Angular position and diffraction line profile

The recorded diffractograms were normalized to unity by dividing each intensity value I(2θ) by the maximum value $I_n = \frac{I(2\theta)}{I_{max}}$. Then, the profile of each diffraction reflection was described by the Pearson VII function according to formula (2):

$$F(2\theta; b, m, a, d, p, q) = a\left[1 + \frac{2\theta - d}{b^2}\right]^{-m} + p \cdot 2\theta + q \tag{2}$$

where:

b, m, a, d, p, q – coefficients determined by the least-squares method

θ – reflection angle [rad.].

The values of coefficients b, m, a, d, p, and q were determined using the least squares method, assuming a linear distribution of the background under the diffraction peak. An example description of the diffraction reflection profile with the determined coefficients is shown in Fig. 2.

Knowledge of the exact functional description of the Bragg reflection was necessary to accurately determine the angular position of each diffraction line. This position is described by a coordinate determining the position of the center of gravity of each reflection (3). This was necessary because the $K_{\alpha 2}$, component, which always causes peak asymmetry, was not removed from the XRD spectrum, so using the position of the reflection maximum would not be accurate enough.

$$2\theta_{sc} = \frac{\int_{2\theta_1}^{2\theta_2} 2\theta : F(2\theta, b, m, a, d, p, q)d(2\theta) - \int_{2\theta_1}^{2\theta_2} 2\theta\,(p \cdot 2a + q) \cdot d(2\theta)}{\int_{2\theta_1}^{2\theta_2} F(2\theta, b, m, a, d, p, q) - \int_{2\theta_1}^{2\theta_2} (p \cdot 2\theta + q) \cdot d(2\theta)} \tag{3}$$

where:

b, m, a, d, p, q – coefficients determined by the least-squares method

θ – reflection angle [rad.].

Furthermore, knowledge of the center of gravity location enabled the determination of the maximum radiation and the exact full width at half maximum (FWHM), which was necessary for further calculations (FULTZ, HOWE 2013).

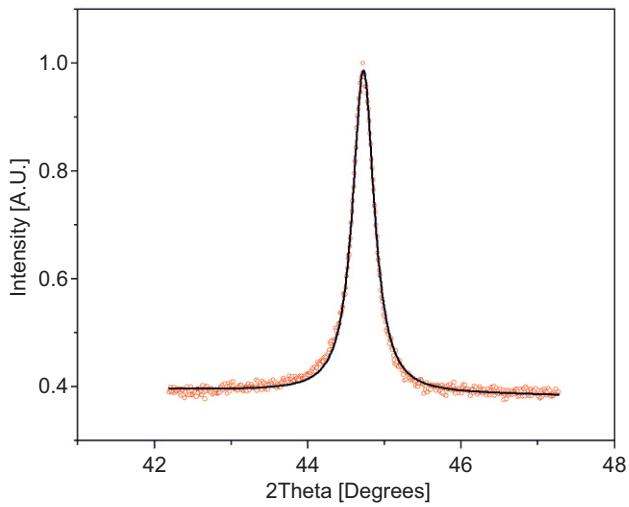

Fig. 2. Peak profile 110
Source: Self-made – own source.

Nelson-Riley Method

The Nelson–Riley extrapolation method was used to determine the crystal lattice parameter, allowing the reduction of systematic errors that depend on the diffraction angle (NELSON, RILEY 1944). For each diffraction peak, an individual lattice parameter a_{hkl} was first calculated using Bragg's law (5). However, these provisional values are affected by angular-dependent errors, which become smaller as the reflection angle θ approaches 90°. Since direct measurement at 2θ = 180° is impossible due to diffractometer geometry, the method uses a correction function $f(\theta)$ (4) that describes how these errors vary with θ. The calculated values a_{hkl} are then plotted as a function of $f(\theta)$. If the assumed form of $f(\theta)$ is correct, the points align approximately along a straight line. Using the least-squares method, the value of the lattice parameter extrapolated to $f(\theta) = 0$ is taken as the final lattice constant a_0 and is presented in Fig. 3 (LIPSON 2001).

$$f(\theta) = \frac{1}{2} \cdot \left(\frac{\cos^2\theta}{\sin\theta} + \frac{\cos^2\theta}{\theta} \right) \tag{4}$$

where:

θ – reflection angle [rad.].

$$a_o = \frac{\lambda \cdot \sqrt{h^2 + k^2 + l^2}}{2 \cdot \sin\theta} \tag{5}$$

where:

h, k, l – Miller index

λ – radiation wave length [Å]

θ – reflection angle [rad.].

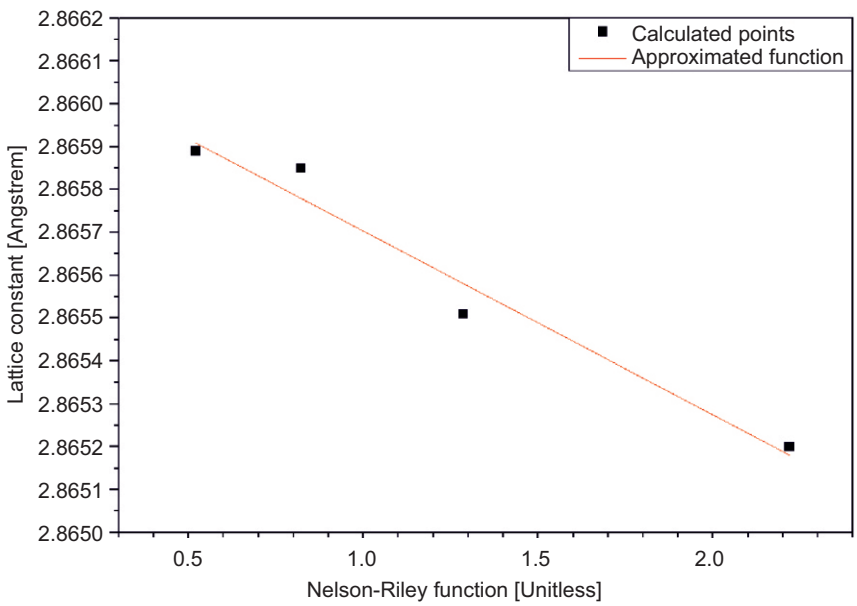

Fig. 3. An example of an approximate crystal lattice function for the tested sample
Source: Self-made – own source.

Scherrer Method

The size of α-iron phase crystallites was determined using the Scherrer method based on the analysis of the half-width of diffraction reflections. The broadening of diffraction lines is directly related to the size of the ordered crystal lattice areas that scatter X-rays in a coherent manner. In the case of smaller crystallites, the diffraction peaks become broader, which allows their quantitative determination

based on the recorded diffraction spectra (SCHERRER 1918, NWAOKAFOR et al. 2021). The effect is described by formula (6).

$$D_v = \frac{K \cdot \lambda}{\beta_r \cdot \cos\theta} \tag{6}$$

D_v – crystallite size perpendicular to the reflecting plane,
K – Scherrer constant equal to 0.9,
λ – wavelength of radiation,
β_r – half-width of the reflection,
θ – reflection angle.

Williamson-Hall Method

The Williamson-Hall method was used to simultaneously evaluate the contribution of crystallite size and lattice distortion (type III stresses) to the broadening of diffraction lines. Unlike the Scherrer method, this method assumes the influence of lattice distortions on the half-width of the reflection (WILLIAMSON, HALL 1953, PELLEG et al. 2005). Assuming this, the relationship can be written as an equation linking the line width to the diffraction angle. After appropriate transformation, a straight function line is obtained, whose slope corresponds to the amount of deformation, and the intercept allows the size of the crystallites to be estimated as shown in Figure 4 (7).

$$\varepsilon = \frac{\beta_z}{4 \cdot \mathrm{tg}\theta} \qquad \beta_z = 4 \cdot \mathrm{tg}\theta \cdot \varepsilon \tag{7}$$

where:
ε – relative lattice distortions,
β_z – reflection width related to the influence of distortions,
θ – reflection angle.

In the Williamson-Hall method, the equation for the half-width of the reflection is (8):

$$\beta = \beta_k + \beta_z \tag{8}$$

β – width of diffraction reflections
β_k – reflection width depending on the size of crystallites
β_z – reflection width with distortion influence

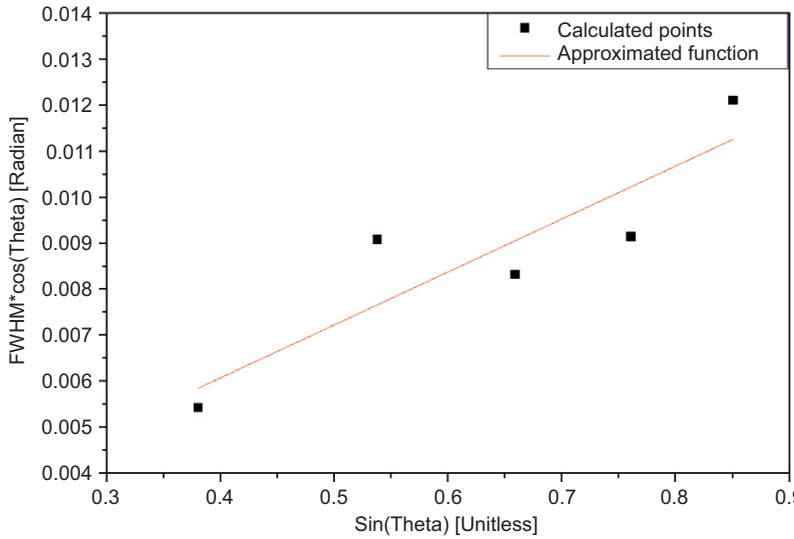

Fig. 4. Approximated function of Williamson-Hall for position x = 0
Source: Self-made – own source.

Results and Discussion

The recorded diffractograms show that a deviation to the "+" side from the center of the focus circle causes significant shifts of the reflections towards higher 2θ angles. In the case of deviations to the "–" side, the opposite is true. Visual analysis of the recorded diffractograms (Fig. 5) indicates a systematic shift in the position of the 2θ peaks depending on the height of the sample.

For each of the diffractograms, measurements were made of the positions of the centers of gravity of the 2θ angle reflections of selected peaks (Tab. 2) and their half-widths were determined (Tab. 3). This is necessary to calculate the size of crystallites or lattice distortions.

Table 2

Measurement of 2θ reflection positions for different sample height settings

Miller Index	X = –1	X = –0.5	X = 0	X = 0.5	X = 1
	[Degrees]	[Degrees]	[Degrees]	[Degrees]	[Degrees]
110	43.941	44.316	44.732	45.087	45.432
200	64.409	64.765	65.106	65.435	65.755
211	81.804	82.101	82.437	82.727	83.008
220	98.550	98.809	99.080	99.356	99.356
310	116.085	116.334	116.549	116.793	116.950

Source: Self-made – own source.

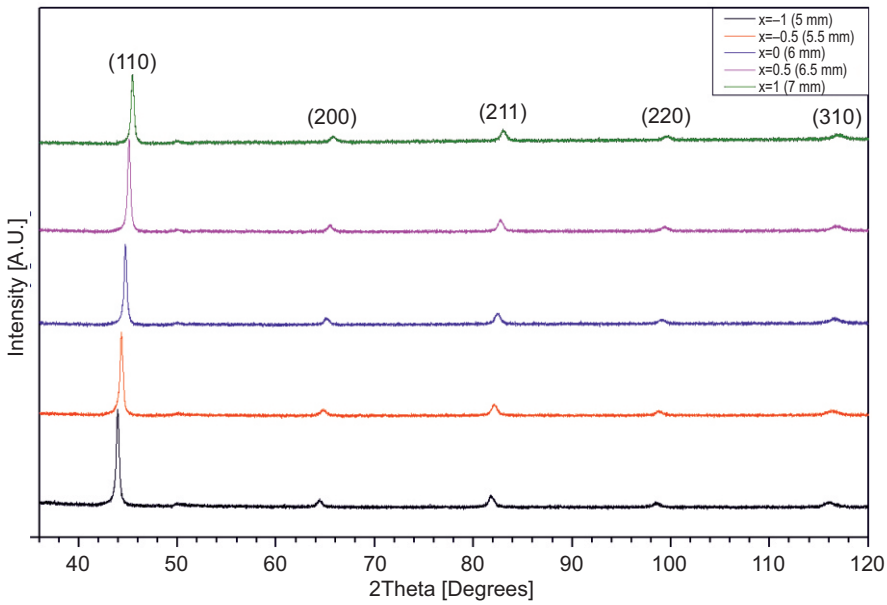

Fig. 5. A comparison of diffractograms with different positions of the samples
Source: Self-made – own source.

Table 3

Measurement of the FWHM of 2θ reflections for different sample height settings

Miller Index	X = –1	X = –0.5	X = 0	X = 0.5	X = 1
	[Degrees]	[Degrees]	[Degrees]	[Degrees]	[Degrees]
110	0.337	0.342	0.336	0.332	0.349
200	0.593	0.720	0.617	0.579	0.683
211	0.670	0.649	0.634	0.628	0.632
220	0.838	0.828	0.807	0.787	0.824
310	1.301	1.316	1.320	1.257	1.356

Source: Self-made – own source.

In addition, the percentage differences of the 2θ angle relative to the correct position were calculated. It can be seen that the largest deviations are for the largest reflection originating from the (110) plane. The data presented in Tables 2 and 4 show that a 1 mm shift of the sample causes a shift of the (110) reflection by as much as approximately 0.8°, while for reflections with a further angle position, this effect is much smaller. A comparison of the shifts for the (110) peak is shown in Figure 6.

Table 4

Differences from the reference position

Miller Index	X = –1	X = –0.5	X = 0	X = 0.5	X = 1
	[Degrees]	[Degrees]	[Degrees]	[Degrees]	[Degrees]
110	–0.791	–0.416	0.000	0.355	0.700
200	–0.697	–0.341	0.000	0.329	0.649
211	–0.633	–0.336	0.000	0.290	0.571
220	–0.530	–0.271	0.000	0.276	0.276
310	–0.464	–0.215	0.000	0.244	0.401

Source: Self-made – own source.

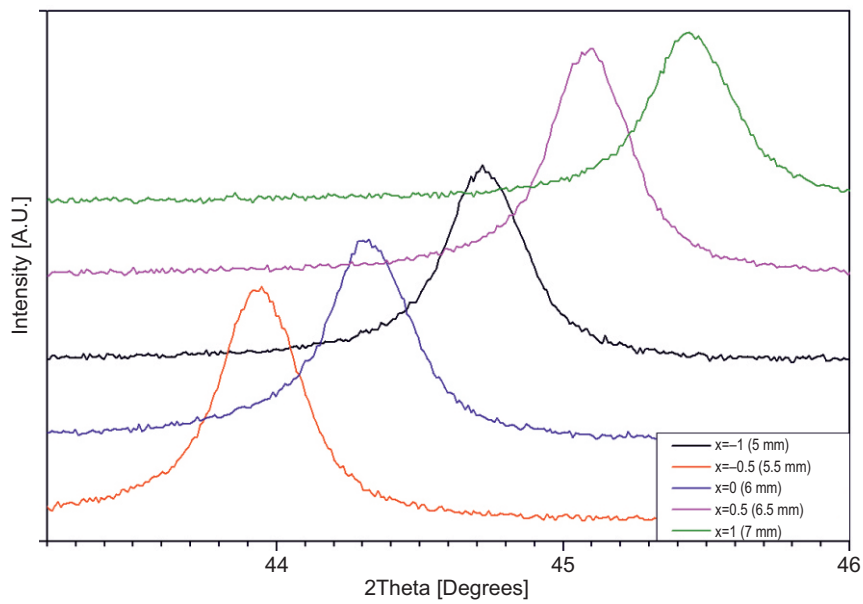

Fig. 6. Overview of peak 110 for different height shifts
Source: Self-made – own source.

The results obtained for the Miller index peak (110) were compared with the theoretical model from equation (1) and summarized in Table 5. The results indicate similar values between the two methods.

Table 6 shows the calculated values of $\sin^2\theta$ for each reflected signal and their ratios relative to the first peak in order to determine the structure layout.

Table 5

Comparison of theoretical values with measured values for peak values with an index of (110)

S[mm]	2θ (Measured) [Degrees]	Measured $\Delta 2\theta$ [Degrees]	Predicted $\Delta 2\theta$ (model) [Degrees]	Measured – predicted [Degrees]
–1	43.941	0.791	0.757	0.034
–0.5	44.316	0.416	0.378	0.038
0	44.732	0.000	0.000	0.000
0.5	45.087	0.355	0.378	0.023
1	45.432	0.700	0.756	0.056

Source: Self-made – own source.

Table 6

Quotient of the values of the sine of theta squared

Measurement	Miller index	2θ	$\sin^2\theta$	$\frac{\sin^2\theta_{hkl}}{\sin^2\theta_{h_1k_1l_1}}$
X = –1 [Degrees]	110	43.941	0.140	1.000
	200	64.409	0.284	2.029
	211	81.804	0.429	3.063
	220	98.55	0.574	4.103
	310	116.085	0.720	5.143
X = –0.5 [Degrees]	110	44.316	0.142	1.000
	200	64.765	0.287	2.049
	211	82.101	0.431	3.081
	220	98.809	0.577	4.119
	310	116.334	0.722	5.074
X = 0 [Degrees]	110	44.732	0.145	1.000
	200	65.106	0.290	2.000
	211	82.437	0.434	2.999
	220	99.08	0.579	3.998
	310	116.549	0.723	4.997
X = 0.5 [Degrees]	110	45.087	0.147	1.000
	200	65.435	0.292	1.988
	211	82.727	0.437	2.971
	220	99.356	0.581	3.955
	310	116.793	0.725	4.935
X = 1 [Degrees]	110	45.432	0.149	1.000
	200	65.755	0.295	1.976
	211	83.008	0.439	2.945
	220	99.356	0.581	3.898
	310	116.95	0.727	4.873

Source: Self-made – own source.

Based on the measurements taken, the lattice constants for each series of measurements were calculated to check for changes between heights. The results are summarized in Table 7 and presented in Figure 7.

Table 7

Results of lattice constants using the N-R method

Position	X = –1	X = –0.5	X = 0	X = 0.5	X = 1
Lattice constant [Å]	2.8678	2.8661	2.8643	2.8653	2.8654

Source: Self-made – own source.

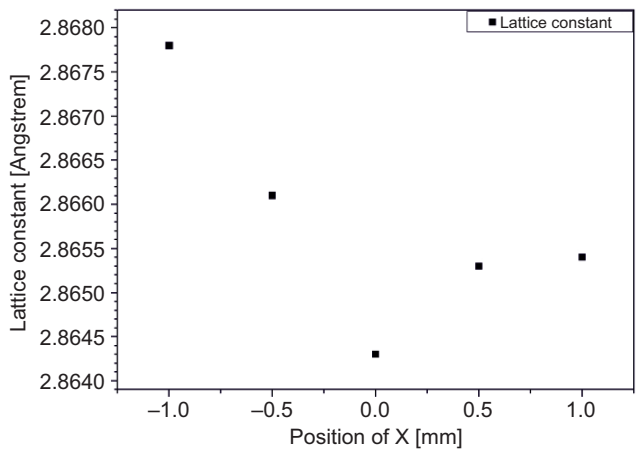

Fig. 7 Lattice constant comparison in the sample shift function
Source: Self-made – own source.

An elementary model of alpha iron with a correct height of 6 mm and a lattice constant calculated using the N-R method. A comparison of the elementary model and the diffractogram for x = 0 is shown in Figure 8.

The next step was to calculate the size of the crystallites using the Scherrer method. The highest value is observed for the (110) peak, and the lowest for the (310) peak. The results are summarized in Table 8.

Table 8

Crystallite sizes determined using the Scherrer method

Miller Index	X = –1 [Å]	X = –0.5 [Å]	X = 0 [Å]	X = 0.5 [Å]	X = 1 [Å]
110	254.401	251.014	255.877	259.291	246.971
200	158.453	130.761	152.878	163.212	138.609
211	157.002	162.447	166.291	168.685	167.980
220	145.421	147.565	151.824	156.722	149.460
310	115.460	114.544	114.543	120.700	112.137

Source: Self-made – own source.

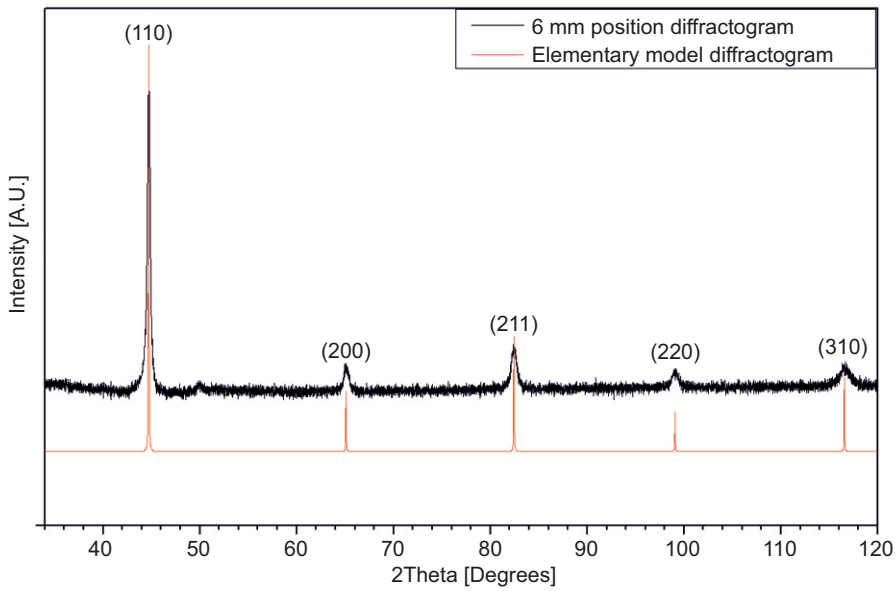

Fig. 8. Comparison of the model diffractogram with the measured diffractogram for x = 0
Source: Self-made – own source.

Additionally, calculations were performed using the W-H method, which also assumes the influence of network distortions. The results obtained using this method were significantly higher. It is also worth noting the lower values for x = –0.5 and x = 1. The results are summarized in Table 9.

Table 9

Results of crystallite size and lattice distortion using the W-H method

W-H	X = –1	X = –0.5	X = 0	X = 0.5	X = 1
D [Å]	992.894	531.411	945.112	910.124	694.838
ε [%]	0.297	0.261	0.288	0.272	0.277

Source: Self-made – own source.

Conclusions

The deviation of the sample position from the center of the circle in Bragg-Brentano geometry focusing causes a systematic shift in the angular positions of the 2θ reflections. Comparing the measurement results with the theoretical model shows that the experiment was performed correctly and that the model accurately determines the possible displacement. The difference between

the measured and calculated results ranged from 0.023 to 0.056 degrees. The calculated lattice constant values varied only within a very small range (2.8643-2.8678 [Å]). This means that the Nelson-Riley method effectively limits the influence of geometric errors on the final result. This effect is most pronounced at the smallest 2θ diffraction angles (e.g., the (110) reflection). For the x = 0 reference setting, the ratios of the calculated $\sin^2\theta_{hkl}$ are close to 1, 2, 3, 4, 5, which confirms their regular (cubic) arrangement. The largest crystallite size was observed for peaks with an index of (110) for the Scherrer method. A relationship between peak size and crystallite size can also be observed, i.e., the larger the peak, the larger the crystallite size. The crystallite size values obtained using the Williamson-Hall method were significantly larger than those calculated using the Scherrer method. This may be due to lattice distortions, although the differences are very large. In summary, the shift causes noticeable changes in the results obtained. Falsifying them can lead to erroneous conclusions and misuse.

Acknowledgements

I would like to thank PhD DSc Eng. Mirosław Bramowicz, for his assistance with the experiment.

References

ASTM E975-13. 2013. *Standard Practice for X-Ray Determination of Retained Austenite in Steel with Near Random Crystallographic Orientation*. ASTM International, West Conshohocken, PA.

Cline J.P., Mendenhall M.H., Black D., Windover D., Henins A. 2015. *The Optics and Alignment of the Divergent Beam Laboratory X-ray Powder Diffractometer and its Calibration Using NIST Standard Reference Materials*. Journal of Research of the National Institute of Standards and Technology, 120: 1-27.

Cullity B.D., Stock S.R. 2014. *Elements of X-Ray Diffraction*, Pearson.

EN 10025-2. 2019. *Hot Rolled Products of Structural Steels – Part 2: Technical Delivery Conditions for Non-Alloy Structural Steels*, European Committee for Standardization (CEN), Brussels.

Fultz B., Howe J.M. 2013. *Transmission Electron Microscopy and Diffractometry of Materials*. Springer.

Harrington G.F., Santiso J. 2021. *Back to Basics Tutorial: X-ray Diffraction of Thin Films*. Journal of Electroceramics, 47: 141-163.

Kriegner D., Matej Z., Kuzel R., Holý V. 2015. *Powder Diffraction in Bragg-Brentano Geometry with Straight Linear Detectors*. Journal of Applied Crystallography, 48: 613-618.

Lipson H. 2001. *The Study of Metals and Alloys by X-Ray Powder Diffraction Methods*. University College Cardiff Press.

Nelson J.B., Riley D.P. 1944. *An Experimental Investigation of Extrapolation Methods in the Derivation of Accurate Unit-Cell Dimensions of Crystals*. Proceedings of the Physical Society, 57: 3-14.

Nwaokafor P., Okeoma K.B., Echendu O.K. 2021. *X-ray Diffraction Analysis of a Class of AlMgCu Alloy Using Williamson–Hall and Scherrer Methods*. Metallography, Microstructure, and Analysis, 10: 727-735.

PELLEG J., ELISH E., MOGILYANSKI D. 2005. *Evaluation of Average Domain Size and Microstrain in a Silicide Film by the Williamson–Hall Method*. Metallurgical and Materials Transactions A, 36: 3187-3194.

SCHERRER P. 1918. *Bestimmung der Größe und der inneren Struktur von Kolloidteilchen mittels Röntgenstrahlen, Nachrichten von der Gesellschaft der Wissenschaften zu Göttingen*. Mathematisch-Physikalische Klasse, 98-100.

WEIDENTHALER C. 2011. *Pitfalls in the Characterization of Nanoporous and Nanosized Materials*. Nanoscale, 3: 792-810.

WILLIAMSON G.K., HALL W.H. 1953. *X-ray Line Broadening from Filed Aluminium and Wolfram*. Acta Metallurgica, 1: 22-31.